Augmented Lagrangian method for angular super-resolution imaging in forward-looking scanning radar

Yuebo Zha
Yulin Huang
Jianyu Yang

Augmented Lagrangian method for angular super-resolution imaging in forward-looking scanning radar

Yuebo Zha,* Yulin Huang, and Jianyu Yang

University of Electronic Science and Technology of China, School of Electronic Engineering, 2006 Xiyuan Road, Gaoxin Western District, Chengdu 611731, China

Abstract. Angular super-resolution imaging in the forward-looking area of a scanning radar platform plays an important role in the application of scanning radar. However, the angular resolution of scanning radar is limited by the system parameters. Thus, improving the angular resolution of scanning radar beyond the limitation of the given system parameters is desired. We present an angular super-resolution imaging method by solving the associated deconvolution problem. We first formulate an angular super-resolution problem in scanning radar as a deconvolution task and then convert it to a constrained optimization problem by incorporating the prior information of the target in the scene. We then solve the constrained optimization problem in convex optimization framework using an augmented Lagrangian method. In order to solve the constrained optimization problem, a corresponding augmented Lagrangian function is constructed and its saddle point is found using alternating direction method. The advantages of the proposed method for angular super-resolution imaging in scanning radar are that the proposed method can not only realize the angular super-resolution imaging in scanning radar but also has high precision. Simulation and experiment results are given at the end to verify the validity of the proposed method compared with a Wiener filter that is applicable for angular super-resolution in scanning radar. © *The Authors. Published by SPIE under a Creative Commons Attribution 3.0 Unported License. Distribution or reproduction of this work in whole or in part requires full attribution of the original publication, including its DOI.* [DOI: 10.1117/1.JRS.9.096055]

1 Introduction

Due to advantages over optical sensing tools, such as robust performance under all-time and all-weather circumstances, radar plays an important role in such realms as earth observation, oceanic monitoring, and military reconnaissance.[1,2] To realize these applications, two-dimensional high resolution is usually required. The high range resolution can be obtained by transmitting the wideband signal and using the pulse compression technique. The high resolution in azimuth/angular can be realized using synthetical aperture technique or Doppler beam sharpening approaches. However, these techniques are unable to realize radar imaging in the forward-looking area of the radar platform. The reason is that the Doppler resolution and the range resolution in the forward-looking area are parallel.[3]

Scanning radar works as a noncoherent sensor, which is suitable for any geometrical situation and is able to realize two-dimensional radar imaging in the forward-looking area of the radar platform. In the same way, the pulse compression provides the high range resolution, while the angular resolution is usually poor when compared with the range resolution. For scanning radar, the upper limit of angular resolution is determined by the effective wavelength and the size of the antenna. Moreover, the angular resolution suffers and degrades as a function of target distance. One method to improve the angular resolution in scanning radar image can be accomplished by

---

*Address all correspondence to: Yuebo Zha, E-mail: zhayuebo@163.com

increasing the physical size of the antenna aperture. However, there may be insufficient space to accommodate such a large size antenna in the application. Therefore, an improvement in the angular resolution of the scanning radar with fixed parameters using signal processing methods is considered.

According to Refs. 4 and 5, the echo of scanning radar can be modeled as the convolution of the transmitted signal with the scattering coefficients of the targets. Therefore, in theory, a deconvolution method can enhance the angular resolution of the scanning radar.[6] Deconvolution aims at removing the transfer function, system noise, and other nonidealities of the imaging process, thereby improving the imaging resolution.[7] The deconvolution approach has been widely used for video restoration,[8] image processing,[9] sparse signal restoration,[10] and through-wall radar imaging,[11] while less work on the deconvolution approach for angular super-resolution imaging in scanning radar has been reported.

This paper presents a deconvolution method for improving the angular resolution of scanning radar. We first convert the angular super-resolution imaging task in scanning radar into an equivalent deconvolution problem. It is well-known that the deconvolution problem is ill-posed, which means the solution to the deconvolution problem is unstable and sensitive to the noise. To stabilize the solution of the deconvolution problem, we must utilize some prior information of the solution to the deconvolution problem. This paper focuses on some applications such as the detection of detecting and city area imaging, and the case where a small number of dominant scatterers are distributed in the scene. In these applications, large coefficients of the scatterers can capture most of the information of the scene.[12] Inspired by the Bayesian compressive sensing,[13] the statistic characteristics of the dominant scatterers in the illuminated scene can be represented by l_1-norm. Then the deconvolution technique for dominant scatterers in angular super-resolution imaging can be converted into the corresponding l_1 optimization problem. Therefore, the l_1 regularization is adopted and the deconvolution problem can be written with a constrained optimization form. Recently, applications of l_1-norm minimization can be found in Ref. 14 for ISAR imaging,[15] for feature enhanced, and for through-wall radar image.[16] In this paper, we are focused on solving the deconvolution problem, which corresponds to the task of angular super-resolution imaging in the forward-looking area of radar platform. Finally, the constrained optimization problem is solved using an augmented Lagrangian method. The rationale behind the augmented Lagrangian method is to find a saddle point of the associated augmented Lagrangian function, which combines the function to be optimized with a Lagrange multiplier term and a penalty term for the constraints.[17] This leads to an alternating direction method for finding the saddle point of the augmented Lagrangian function. Compared with the traditional Lagrangian multiplier method, the augmented Lagrangian method overcomes numerical difficulties due to the penalty going to infinity.[18] Based on simulation and experimental results, we demonstrate that the proposed deconvolution algorithm has better angular super-resolution performances.

The rest of this paper is organized as follows: Sec. 2 presents the signal model for scanning radar and converts the angular super-resolution problem into an equivalent deconvolution problem. Section 3 presents an augmented Lagrangian method to solve the corresponding deconvolution problem. In Sec. 4, simulation and experimental results are given to demonstrate the validity of the proposed method. Finally, the conclusions are given in Sec. 5.

2 Signal Model for Scanning Radar in Azimuth

In this section, we introduce the signal model for scanning radar and convert the angular super-resolution problem into an equivalent deconvolution problem. The details of the deconvolution algorithm for the angular super-resolution problem will be subsequently provided.

Suppose that the radar works in the scanning mode. The geometrical model of scanning radar is illustrated in Fig. 1. The radar platform at the altitude H is moving along the Y-axis corresponding to the range direction, while the antenna scans the scene along the X-axis corresponding to the azimuth direction with constant angular velocity ω and then receives the echo data from the observed scene. Assume that the target in the azimuth can be considered as an ideal point. For an isolated target scatter, the received signal at the receiver output is proportional to the
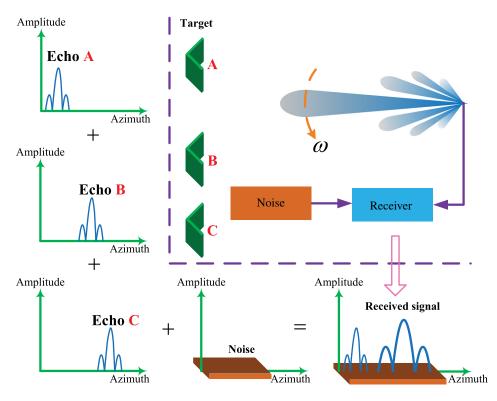
Fig. 1 The geometrical model of the scanning radar.

antenna pattern. The left part of Fig. 1 shows that the scanning radar collects echo data, while it scans in the azimuth across the target field. It is noted that the adjacent echoes mostly cover the same target features on the observed scene but with different contributions to the overall signal, which is shown in the bottom part of Fig. 1.

At first, the conventional range compression and range migration correction are applied to the echo data with the current approaches.[2,19] The range compression and range migration to correct data are denoted by $g(\theta, \varphi, r)$, where r is the slant range from the radar to the target and θ, φ denote the angle between the direction of the antenna to the target and flight direction and the incident angle of the beam, respectively, which are smaller than 10 deg. On the other hand, it is assumed that the antenna pattern is of relative isotropy to the imaging scene. Then the received signal of the scanning radar along the range profile can be recognized as a convolution kernel comprising the antenna power pattern in the angle coordinates and the pulse modulation function in the range dimension,[20] which could be expressed as

$$g(\varphi, \theta, r) = f(\varphi, \theta, r) * \left[a(\varphi, \theta) x \left(\frac{2r}{c} \right) \right], \tag{1}$$

where $*$ denotes the convolution operator, $g(\varphi, \theta, r)$ is the received signal of the scanning radar after range compression and range cell migration, $f(\varphi, \theta, r)$ is the effective scattering coefficient, $a(\varphi, \theta)$ is the antenna pattern, $x(2r/c)$ denotes the pulse modulation function, and c represents the speed of light.

Without loss of generality, we consider the variation in scattering with the azimuth angle θ for a fixed range r_0 and a fixed angle φ. Note that with the limited range resolution, the range averaging scattering would be exactly equal to the effective scattering evaluated at the range of the interested r_0. Thus, we only consider the azimuth variation in Eq. (1) that can be written as

$$g(\varphi_0, \theta, r_0) = f(\varphi_0, \theta, r_0) * \left[a(\varphi_0, \theta) x \left(\frac{2r_0}{c} \right) \right]. \tag{2}$$

For mathematical simplicity, we only consider the azimuth variation. Then we can rewrite Eq. (2) as

$$g(\theta) = f(\theta) * a(\theta). \tag{3}$$

In addition, the presence of the noise contaminates the data $g(\theta)$. The formation of the data $g(\theta)$ can be described as

$$g(\theta) = f(\theta) * a(\theta) + n(\theta), \tag{4}$$

where $n(\theta)$ represents the noise.

In the case of observing a certain scene Ω, the echo returned to the radar is the whole scene. The reflectivity of Ω can be denoted as a two-dimensional matrix

$$\Omega = \begin{bmatrix} f(\varphi_1, \theta_1), & f(\varphi_1, \theta_2), & \cdots & f(\varphi_1, \theta_A) \\ f(\varphi_2, \theta_1), & f(\varphi_2, \theta_2), & \cdots & f(\varphi_2, \theta_A) \\ \vdots & & \ddots & \vdots \\ f(\varphi_R, \theta_1), & f(\varphi_R, \theta_2), & \cdots & f(\varphi_R, \theta_A) \end{bmatrix}_{R \times A}, \tag{5}$$

where R represents the discretization cells of the scene in the range direction, and A denotes the discretization cells of the scene in the azimuth direction.

To attain the corresponding discrete convolution equation, we represent the scene Ω as a vector by stacking the columns of the matrix:

$$\begin{aligned} f &= \mathbf{vec}(\Omega) \\ &= [f(\varphi_1, \theta_1) \quad \ldots \quad f(\varphi_1, \theta_A), \ f(\varphi_2, \theta_1) \quad \ldots \quad f(\varphi_2, \theta_A), \quad \cdots, \ f(\varphi_R, \theta_1) \quad \ldots \quad f(\varphi_R, \theta_A)]^T, \end{aligned} \tag{6}$$

where $\mathbf{vec}$ maps $\Omega^{R \times A}$ to $\Omega^{RA \times 1}$ by stacking the rows of a matrix in a vector, and $[\cdot]^T$ is used for the matrix-vector transposition. Likewise,

$$g = [g(\varphi_1, \theta_1) \quad \ldots \quad g(\varphi_1, \theta_A), \ g(\varphi_2, \theta_1) \quad \ldots \quad g(\varphi_2, \theta_A), \quad \cdots, \ g(\varphi_R, \theta_1) \quad \ldots \quad g(\varphi_R, \theta_A)]^T \tag{7}$$

and

$$n = [n(\varphi_1, \theta_1) \quad \ldots \quad n(\varphi_1, \theta_A), \ n(\varphi_2, \theta_1) \quad \ldots \quad n(\varphi_2, \theta_A), \quad \cdots, \ n(\varphi_R, \theta_1) \quad \ldots \quad n(\varphi_R, \theta_A)]^T. \tag{8}$$

According to Ref. 21, a discrete convolution equation corresponding to Eq. (4) can be written as

$$g = Hf + n, \tag{9}$$

where g, f, and n are of dimension $AR \times 1$, and H is of dimension $AR \times AR$ and is ordered as

$$H = \begin{bmatrix} H_1 & H_R & \cdots & H_2 \\ H_2 & H_1 & \cdots & H_3 \\ \vdots & \vdots & \ddots & \vdots \\ H_R & H_{R-1} & \cdots & H_1 \end{bmatrix}_{RA \times RA}. \tag{10}$$

The matrix H is a block circulant consisting of circulant blocks with dimensions $RA \times RA$. Each partition of $H_i (i = 1, 2, \cdots R)$ has the size $A \times A$, which is constructed from the i'th scanning antenna pattern. Each partition H_i can be written as

$$H_i = \begin{bmatrix} a(\theta_1, \varphi_i) & a(\theta_A, \varphi_i) & \cdots & a(\theta_2, \varphi_i) \\ a(\theta_2, \varphi_i) & a(\theta_1, \varphi_i) & \cdots & a(\theta_3, \varphi_i) \\ a(\theta_3, \varphi_i) & a(\theta_2, \varphi_i) & \cdots & \\ \vdots & \vdots & \ddots & \vdots \\ a(\theta_A, \varphi_i) & a(\theta_{A-1}, \varphi_i) & \cdots & a(\theta_1, \varphi_i) \end{bmatrix}_{A \times A}. \tag{11}$$

The goal of angular super-resolution in scanning radar is to infer f from the g, as accurately as possible. This task is called the deconvolution problem in this paper. The challenge is that the data g recorded at the output of the radar system are a low-pass-filtered version of the original data f due to the "low-pass" filtering effect of the antenna. So the high-frequency parts of the g are lost by the antenna, which leads to the decrease of the azimuth resolution of the scanning radar system.

3 Augmented Lagrangian Solver for Angular Super-Resolution Imaging

In this section, we first analyze the phenomenon of noise amplification in the conventional inverse filter methods for solving a deconvolution problem. The deconvolution problem is converted into a constrained optimization task. Then the augmented Lagrangian method is presented as the foundation of the following deconvolution method. Finally, the angular super-resolution is realized by solving the constrained optimization via augmented Lagrangian method.

3.1 *Deconvolution Problem and Constrained Optimization Problem*

The conventional linear deconvolution method would be a simple division of data g by the transferring function in the Fourier domain. Using the Fourier transform, Eq. (4) can be written as

$$G(w) = H(w)F(w) + N(w), \tag{12}$$

where $G(w)$, $H(w)$, $F(w)$, and $N(w)$ are the Fourier transforms of g, h, f, and n, respectively. The linear deconvolution approach can be stated as the task of finding a linear operator T such as

$$\hat{F}(w) = \frac{G(w)}{T(w)} = F(w) + \frac{N(w)}{H(w)}. \tag{13}$$

The challenge consists in that the convolution in the Fourier corresponds to multiplication while the deconvolution is Fourier division. For a radar system, the multipliers are often small for high frequencies, and the inverse filter $1/T(w)$ is large when $T(w)$ is very small. This results in large noise amplification, thus the angular super-resolution performance might be degraded. In order to solve the deconvolution problem, we employ the framework of regularization theory which provides the most likely solution given the recorded data and a reasonable assumption of the true scene. The details of the proposed methods are presented next.

To perform the deconvolution, we employ the framework of regularization theory, which not only suppresses the noise amplification but also allows for solutions that reflect reality. Regularization theory allows us to incorporate the prior information about the targets. In order to apply the regularization theory to the deconvolution problem, we first transform the deconvolution problem into an equivalent constrained optimization problem by adding the prior information of the targets.

In some applications of radar imaging, such as detection of ocean ships and aircraft monitoring, the number of dominant scattering targets is much smaller than the number of the overall samples. Therefore, the few large coefficients of the scatterers can capture most of the information of the scene while the weak scattering center is regarded as the noise in the radar imaging.[12]

Considering the points that lie on the constant l_1-norm curve, the ones with two coordinates having equal magnitudes are favored by minimization of the l_k-norm.[22] The effect of the l_1-norm favors a field with smaller number of dominant scatterers and better preserves the scatterers and their magnitudes. The deconvolution problem can be solved by constrained optimization based

on l_1-norm. Finally, the regularization theory for angular super-resolution by solving the corresponding deconvolution problem leads to the following constrained optimization problem:

$$\arg \min_{f} \|Lf\|_1 \quad \text{subject to:} \|g - Hf\|_2^2 \le \varepsilon, \tag{14}$$

where L denotes a discrete approximation of a regularization operator and $\varepsilon \ge 0$ is a parameter which depends upon the noise variance.

Equation (14) can be written as an equivalent unconstrained optimization problem, which yields the following equation:

$$\arg \min_{f} \lambda\|Lf\|_1 + \frac{1}{2}\|g - Hf\|_2^2. \tag{15}$$

It should be noted that the problem in Eq. (15) can be seen as the Lagrangian problem [Eq. (14)]. From the optimization, the solution of Eq. (15) well approximates that of Eq. (14) only when λ becomes large, which results in difficulty in numerically solving the equation. To avoid λ going to infinity, the augmented Lagrangian method is used to solve Eq. (15), which avoids numerical instabilities that would occur as $\lambda \to \infty$. The details of this approach are presented next.

3.2 *General Framework of Augmented Lagrangian Method*

In this section, the general framework of the augmented Lagrangian method is presented as the foundation of the following discussion. The basic idea of the augmented Lagrangian method goes back to the work of Gabay and Mercier[23] and Glowinski and Marocco.[24]

Considering an unconstrained optimization problem of the form

$$\arg \min_{f} \{\theta_1(Lf) + \theta_2(Hf)\}, \tag{16}$$

where θ_1 and θ_2 are the convex functions and L is the continuous linear operator. By introducing an auxiliary variable $z = \begin{bmatrix} u \\ v \end{bmatrix}$, to serve as the augment of θ_1 and θ_2, under the constraint of $z = \begin{bmatrix} H \\ L \end{bmatrix} f$, Eq. (16) can be transformed into an equivalent constrained optimization problem as follows:

$$\arg \min_{f,z} \{\theta_1(v) + \theta_2(u)\} \quad \text{subject to:} \begin{bmatrix} u \\ v \end{bmatrix} = \begin{bmatrix} H \\ L \end{bmatrix} f. \tag{17}$$

Therefore, the augmented Lagrangian function associated with Eq. (17) is defined as

$$L_A(f, u, v, \gamma_u, \gamma_v) = \theta_1(v) + \theta_2(u) + \gamma_v^T(v - Lf) + \gamma_u^T(u - Hf)$$
$$+ \frac{\rho_v}{2}\|v - Lf\|_2^2 + \frac{\rho_u}{2}\|u - Hf\|_2^2, \tag{18}$$

where γ_u and γ_v are the vectors of Lagrange multipliers, and ρ_u and ρ_v are called the penalty parameters.[25]

The idea of the augmented Lagrangian method is to find a saddle point of $L_A(f, u, v, \gamma_u, \gamma_v)$, which is also the solution to the original problem in Eq. (16). Then the saddle point of the augmented Lagrangian function [Eq. (18)] can be found using the alternating direction method, which results in the iterative scheme in Table 1.

The convergence of the augmented Lagrangian method is guaranteed by the theorem in Ref. 26. The augmented Lagrangian method has been recently used for an imaging inverse problem.[25,27] In Ref. 8, the augmented Lagrangian method is used to restore video. It is also studied in computed tomography.[28] In the following, we apply the idea of the augmented Lagrangian method to solve Eq. (14).

Table 1 Augmented Lagrangian method.

Augmented Lagrangian method for Eq. (18)

Input: Set $k = 0$, started at ρ_u, ρ_v, u_k, v_k, $(\gamma_u)_k$ and $(\gamma_v)_k$

Repeat

Step 1: $f_{k+1} = \arg\min\limits_f \left\{ \begin{bmatrix} (\gamma_v)_k \\ (\gamma_u)_k \end{bmatrix}^T \begin{bmatrix} v_k - Lf \\ u_k - Hf \end{bmatrix} + \left\| \begin{bmatrix} \sqrt{\frac{\rho_v}{2}}(v_k - Lf) \\ \sqrt{\frac{\rho_u}{2}}(u_k - Hf) \end{bmatrix} \right\|_2^2 \right\}$

Step 2: $v_{k+1} = \arg\min\limits_v \{\theta_1(v) + [(\gamma_v)_k]^T(v_k - Lf_{k+1}) + \frac{\rho_v}{2}\|v - Lf_{k+1}\|_2^2\}$.

Step 3: $u_{k+1} = \arg\min\limits_u \{\theta_2(u) + [(\gamma_u)_k]^T(u_k - Hf_{k+1}) + \frac{\rho_u}{2}\|u - Hf_{k+1}\|_2^2\}$.

Step 4: $(\gamma_v)_{k+1} = (\gamma_v)_k - \rho_v(v_{k+1} - Lf_{k+1})$.

Step 5: $(\gamma_u)_{k+1} = (\gamma_u)_k - \rho_u(u_{k+1} - Hf_{k+1})$.

Step 6: $k = k + 1$.

Until stopping criterion is satisfied.

3.3 *Applying Augmented Lagrangian Method to Deconvolution Problem*

Starting from Eq. (14), we introduce auxiliary constraint variables u and v. The unconstrained optimization problem [Eq. (14)] can be written in the form of Eq. (17) as

$$\theta_1(f) = \lambda\|Lf\|_1 \quad \theta_2(Hf) = \frac{1}{2}\|g - Hf\|_2^2 \quad u = Hf, v = Lf. \tag{19}$$

The unconstrained optimization problem is

$$\arg\min_{f,u,v}\{E(f,u,v) = \lambda\|v\|_1 + \frac{1}{2}\|g - u\|_2^2\} \quad \text{subject to:} u = Hf, \quad v = Lf. \tag{20}$$

The authors of Refs. 27 and 29 have also utilized this method in the context of imaging restoration. However, our emphasis here is on angular super-resolution in scanning radar. Before processing, we rewrite Eq. (17) concisely as

$$\arg\min_z E(z) \quad \text{subject to:} z = Cf, \tag{21}$$

where $z = \begin{bmatrix} u \\ v \end{bmatrix}$ and $C = \begin{bmatrix} H \\ L \end{bmatrix}$. Since Eq. (21) is equivalent to Eq. (14), solving Eq. (21) with respect to f yields the desired radar image with angular super-resolution.

The augmented Lagrangian equation associated with Eq. (21) is

$$L_A(f,z,\gamma) = E(z) + \gamma^T(z - Cf) + \frac{\mu}{2}\left\|z - Cf\right\|_2^2, \tag{22}$$

which combines a multiplier term $\gamma^T(z - Cf)$ with Lagrangian multipliers $\gamma \triangleq [\gamma_u^T, \gamma_u^T]^T$ and a quadratic penalty term $\mu/2\|z - Cf\|_2^2$.[28] For easier manipulation, the multiplier term can be absorbed into the penalty term in Eq. (22), which leads to the following equation:

$$L_A(f,z,\gamma) = E(z) + \frac{\mu}{2}\|z - Cf - \eta\|_2^2 + \text{const}, \tag{23}$$

where $\eta \triangleq [\eta_u^T, \eta_v^T]^T = (-1/\mu)\gamma$ is a constant independent of f and z, and $\text{const} = (-\mu/2)\|\eta\|_2^2$.

Next, we find the saddle point of Eq. (23) using the alternating direction method shown in Table 1, which results in the following equations:

$$f_{k+1} = \arg\min_f\left\|z_k - Cf - \eta_k\right\|_2^2, \tag{24}$$

$$z_{k+1} = \arg \min_{z} E(z) + \frac{\mu}{2} \left\| z - Cf_{k+1} - \eta_k \right\|_2^2, \tag{25}$$

$$\eta_{k+1} = \eta_k - (z_{k+1} - Cf_{k+1}). \tag{26}$$

We now solve these equations one by one.

3.3.1 *f-subproblem*

By dropping the index k, the solution of Eq. (24) is found by considering the normal equation as follows:

$$C^T C f = C^T (z_k + \eta_k), \tag{27}$$

or, equivalently,

$$(H^T H + L^T L) f = H^T [u_k + (\eta_u)_k] + [v_k + (\eta_v)_k]. \tag{28}$$

The convolution matrix H in Eq. (28) is a Block Toeplitz matrice, with each element of it being the Toeplitz block structure. This leads to an efficient solution for Eq. (28) using the pre-conditioned conjugate gradient method. Therefore, Eq. (28) has the following solution:

$$f = \mathfrak{F}^{-1} \left\{ \frac{\mathfrak{F}(H)^T \mathfrak{F}[u_k + (\eta_u)_k] + \mathfrak{F}[v_k + (\eta_v)_k]}{\mathfrak{F}(H)^T \mathfrak{F}(H) + \mathfrak{F}(L)^T \mathfrak{F}(L)} \right\}, \tag{29}$$

where $\mathfrak{F}$ represents the Fourier transform operator. The matrix $\mathfrak{F}(H)$ can be precalculated outside the main loop. In application where a high number of data are collected, the computation burden of the method is primarily determined by how Eq. (29) is solved, which in turn requires only one forward FFT and one inverse FFT per iteration. Therefore, at each iteration, the main complexity of solving Eq. (28) is in the order of $\mathcal{O}(AR \log A)$ operations.

3.3.2 *z-subproblem*

We see that due to the structure of $E(z)$ and C, Eq. (25) can be separated into the following parts:

$$u_{k+1} = \arg \min_{u} \left\{ \frac{1}{2} \|g - u\|_2^2 + (\gamma_u^T)_k (u - Hf_{k+1}) + \frac{\mu}{2} \|u - Hf_{k+1}\|_2^2 \right\}, \tag{30}$$

$$v_{k+1} = \arg \min_{v} \left\{ \lambda \|v\|_1 + (\gamma_v^T)_k (v - f_{k+1}) + \frac{\mu}{2} \left\| v - f_{k+1} \right\|_2^2 \right\}. \tag{31}$$

Equations (30) and (31) are independent of each other and can be solved simultaneously. Equation (30) is quadratic and has a closed solution.

$$u_{k+1} = (1 + \mu)^{-1} [\mu Hf_{k+1} + g - (\eta_u)_k]. \tag{32}$$

According to Ref. 30, Eq. (31) can be solved using the shrinkage equation. Then, Eq. (31) becomes

$$v_{k+1} = \mathrm{shrink}_{\frac{\lambda}{\mu}}[v_k - f_{k+1} - (\eta_v)_k]$$
$$= \frac{v_k - f_{k+1} - (\eta_v)_k}{\|v_k - f_{k+1} - (\eta_v)_k\|_2} \times \max \left\{ \|v_k - f_{k+1} - (\eta_v)_k\|_2 - \frac{\lambda}{\mu}, 0 \right\}, \tag{33}$$

where $0 \cdot (0/0) = 0$ is assumed.

Finally, the parameter η_u and η_v are updated as

$$(\eta_u)_{k+1} = (\eta_u)_k - (u_{k+1} - Hf_{k+1}), \tag{34}$$
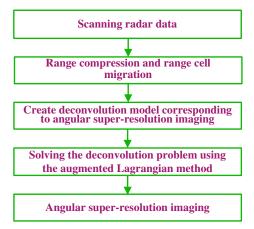
Fig. 2 The flowchart of the presented deconvolution algorithm for angular super-resolution imaging.

$$(\eta_v)_{k+1} = (\eta_v)_k - (v_{k+1} - f_{k+1}). \tag{35}$$

To make this clear, the main flowchart of the proposed decovolution algorithm for angular super-resolution in scanning radar is shown in Fig. 2.

4 Experimental Results

In order to show the validity of the proposed deconvolution method for angular super-resolution in scanning radar, simulation and experimental results are presented in this section.

4.1 Simulations

In this section, the simulation results are presented to demonstrate the performance of the proposed deconvolution method for angular super-resolution in scanning radar. The simulation scene is shown in Fig. 3. The results are compared with those obtained by the Wiener filter method and the operator L is chosen as the I, where I represents the identity matrix. In the tests, the iteration was manually adjusted to yield the best angular super-resolution result for each experimental condition. To get the final result of the solution, the parameter μ is essential. The issue of how to optimally select μ is important, but is outside of the scope of this work. In this paper, the parameter is set as 10 for all simulations and experiments according to the method from the authors of Ref. 31.

Some related scanning radar system parameters are set as follows: the radar carrier frequency is 10 GHz and the pulse repetition frequency is 4000 Hz with an antenna scanning speed 20 deg /s. The bandwidth of the transmitted signal is 2 MHz and the 3-dB width of the real beam is about 3 deg.

In order to quantify and compare the angular super-resolution performance of the proposed deconvolution method on the simulation data, relative error (ReErr),[32] structure similarity (SSIM),[33] and the peak-to-valley point difference in decibels are used in the simulations. They are defined as follows:

$$\text{ReErr} = \frac{\left\| \hat{f} - f \right\|_2}{\left\| f \right\|_2}; \qquad \text{SSIM} = \frac{2\rho_{(\hat{f},f)} \cdot (2\mu_{\hat{f}} \cdot \mu_f)}{(\mu_{\hat{f}}^2 + \mu_f^2)(\sigma_{\hat{f}}^2 + \sigma_f^2)}, \tag{36}$$

where μ, σ, and ρ are the mean, standard deviation of the vectors, and the correlations corresponding to the vectors f and $\hat{f}$. $\hat{f}$ and f represent the obtained angular super-resolution result and the original targets, respectively. The SSIM is a quality measurement between the
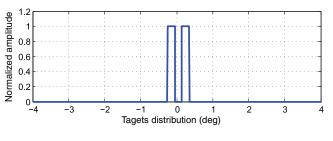
Fig. 3 Simulation scene.

super-resolution result and the original scene. The value of SSIM is between -1 and 1, and 1 denotes full identification with the original scene. The peak-to-valley point difference in decibels is defined in Fig. 4 and quantifies the ability of an angular super-resolution algorithm to separate two closely spaced targets. The difference of the peak-to-valley point in decibels is between 0 and $-\infty$, where 0 means that the angular super-resolution algorithm can fully separate two closely spaced targets.

In order to show the angular super-resolution performance of the proposed method, we simulate the case of different signal-to-noise ratios (SNRs). Figure 5 shows the angular super-resolution results by using the proposed method and Wiener filter approach under different noise levels. Figure 6 shows the evolution of the ReErr and the SSIM with different SNRs. Some observations can be made based on the results in Figs. 5 and 6. For the isolated target, the echo is proportional to the antenna pattern. The echo of two adjacent targets is added and form a single peak as illustrated in Fig. 5. Hence, the individual response cannot be distinguished. The second row of Fig. 5 is the angular super-resolution results obtained by the Wiener filter method, and the third row of Fig. 5 represents the angular super-resolution results given by the proposed deconvolution method. In Fig. 6, the ReErr, whose ideal value is 0, is shown. When the value of the ReErr gets smaller, the precision of the angular super-resolution method increases. The metric SSIM is a quality measurement between the angular super-resolution result and the original scene. The value of SSIM is between -1 and 1, where 1 means the angular super-resolution result that fully identifies with the original scene. This leads to the larger value of the SSIM and a better performance of the proposed angular super-resolution method in terms of quality. It is clear that the proposed deconvolution method gives better results than the Wiener filter method. For example, in the case of SNR $= 10$ dB, the angular super-resolution result of our method not only seems more appealing, but also has a better performance in terms of ReErr and SSIMs.
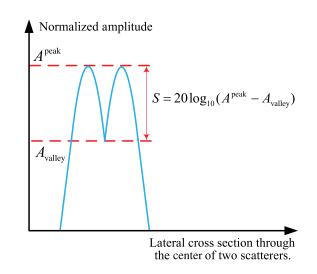

Fig. 4 The definition of the peak-to-valley point difference in decibels.
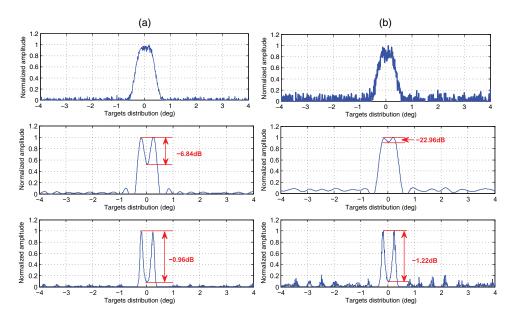
Fig. 5 The results of the angular super-resolution. From top to bottom, you can see the received echo under different Gaussian noise levels and the angular super-resolution results obtained using the Wiener filter and the proposed method, respectively: (a) the noise level is 20 dB; and (b) the noise level is 10 dB.
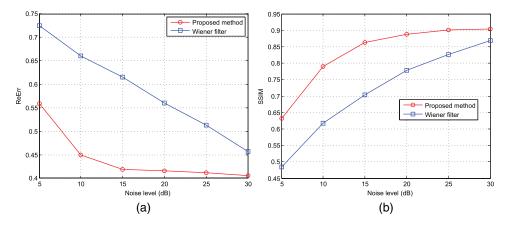

Fig. 6 Evolution of the ReErr and SSIM along the noise SNRs for the simulations.
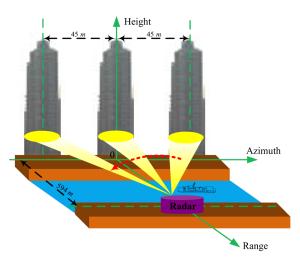

Fig. 7 The tested scene.

4.2 Experimental Results

In order to show the effectiveness of the proposed deconvolution algorithm for angular super-resolution in scanning radar, the real data results are presented. Figure 7 shows the three buildings and their distributions. The range between the scene center and the radar is about 594 m and the distance of each building is 45 m. The transmitted antenna pattern is obtained through the measurement result in the microwave anechoic chamber in the University of Electronic Science and Technology of China. However, due to the noise and energy degradation in actual situations, the antenna pattern used in deconvolution is not consistent with the transmitted pattern. To achieve nice results, we use a pretreatment for the antenna pattern which changes the length of the sidelobe while retaining the width of the main beam of the original pattern. The width of the sidelobe is changed step by step and is chosen by the best experiment result for random data in one scan. In our experiment for scene data processing, this method for choosing the appropriate antenna pattern is effective. The echo from the three buildings is much stronger than that from other areas so that the scene can be considered as the combination of three point targets. Employing the scanning radar system in Fig. 8, the data are acquired. The scanning radar system parameters for the experiment are listed in Table 2.

Compared with the Wiener filter result, the proposed method yields a greater radar image quality with increased resolution, as shown in Fig. 9. Different rows in Fig. 9 correspond to the imaging result with the azimuth profile of the target scene. The first row of Fig. 9 shows the scanning radar image. The image cannot distinguish the positions of the buildings. Compared with the second row of Fig. 9, the third row shows the improved angular resolution and higher visual quality. The reason is that the prior information of the target is used in the proposed method, while the Wiener filter method uses no prior information of targets. Therefore, the proposed method is more effective compared with the Wiener filter method.

(a)   (b)

Fig. 8 The scanning radar system [(a) front side and (b) back side] utilized to collected scattering data.

Table 2 Experimental parameters for real data.

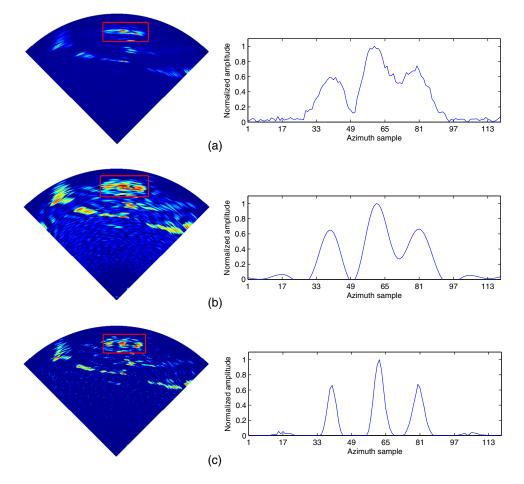| Parameters	Value	Units
Carrier frequency	10	GHz
Bandwidth	30	MHz
Pulse duration	2	μs
Pulse repetition frequency	200	Hz
Antenna scanning velocity	70	deg /s
Antenna scanning area	−45 to +45	deg
Main-lobe beam width	5	deg

Fig. 9 Radar imaging results of real data: (a) the scanning radar image and the azimuth profile of the target area, respectively. (b) The angular super-resolution imaging result via the Wiener filter and the corresponding profile of the target area, respectively. (c) The angular super-resolution imaging result via the proposed method and the corresponding profile of the target area, respectively.

5 Conclusion

This paper presents a deconvolution algorithm for angular super-resolution in scanning radar. After presenting and analyzing the signal model of the scanning radar, we first convert the angular super-resolution problem into an equivalent deconvolution problem. In order to overcome the ill-posed nature of the deconvolution problem, the deconvolution problem is converted into a constrained optimization problem by incorporating the prior information about the targets. Finally, the constrained optimization problem is solved in the framework of the augmented Lagrangian method. Compared with the conventional Wiener filter method, the presented deconvolution algorithm improves the angular super-resolution performance of the scanning radar in terms of precision. Simulations and experimental results show a better performance of the presented method compared with the traditional Wiener filter method. However, there are still some issues that need to be studied in angular super-resolution based on the deconvolution method. Future work will study the robustness of the deconvolution algorithm for angular super-resolution under low SNR levels.

References

1. D. L. Mensa, *High Resolution Radar Cross-Section Imaging*, Vol. 1, p. 280, Artech House, Boston, MA (1991).
2. D. R. Wehner, *High Resolution Radar*, Vol. 1, p. 484, Artech House, Norwood, MA (1987).

3. X. Qiu, D. Hu, and C. Ding, "Some reflections on bistatic SAR of forward-looking configuration," *IEEE Geosci. Remote Sens. Lett.* **5**(4), 735–739 (2008).

4. M. A. Richards, "Iterative noncoherent angular superresolution [radar]," in *Proc. 1988 IEEE National Radar Conf., 1988*, pp. 100–105, IEEE (1988).

5. M. T. Alonso, P. López-Dekker, and J. J. Mallorqui, "A novel strategy for radar imaging based on compressive sensing," *IEEE Trans. Geosci. Remote Sens.* **48**(12), 4285–4295 (2010).

6. M. Migliaccio and A. Gambardella, "Microwave radiometer spatial resolution enhancement," *IEEE Trans. Geosci. Remote Sens.* **43**(5), 1159–1169 (2005).

7. S. Shah, "Deconvolution algorithms for fluorescence and electron microscopy," PhD Thesis, The University of Michigan (2006).

8. S. H. Chan et al., "An augmented Lagrangian method for total variation video restoration," *IEEE Trans. Image Process.* **20**(11), 3097–3111 (2011).

9. M. S. Almeida and M. A. Figueiredo, "Deconvolving images with unknown boundaries using the alternating direction method of multipliers," *IEEE Trans. Image Process.* **22**(8), 3074–3086 (2013).

10. C. Soussen et al., "From Bernoulli–Gaussian deconvolution to sparse signal restoration," *IEEE Trans. Signal Process.* **59**(10), 4572–4584 (2011).

11. K. Browne, R. Burkholder, and J. Volakis, "Fast optimization of through-wall radar images via the method of Lagrange multipliers," *IEEE Trans. Antenna Propag.* **61**(1), 320–328 (2013).

12. S.-J. Wei et al., "Sparse reconstruction for SAR imaging based on compressed sensing," *Prog. Electromagn. Res.* **109**, 63–81 (2010).

13. S. Ji, Y. Xue, and L. Carin, "Bayesian compressive sensing," *IEEE Trans. Signal Process.* **56**(6), 2346–2356 (2008).

14. L. Zhang et al., "High-resolution ISAR imaging by exploiting sparse apertures," *IEEE Trans. Antenna Propag.* **60**(2), 997–1008 (2012).

15. M. Çetin and W. C. Karl, "Feature-enhanced synthetic aperture radar image formation based on nonquadratic regularization," *IEEE Trans. Image Process.* **10**(4), 623–631 (2001).

16. K. E. Browne and R. J. Burkholder, "Nonlinear optimization of radar images from a through-wall sensing system via the Lagrange multiplier method," *IEEE Geosci. Remote Sens. Lett.* **9**(5), 803–807 (2012).

17. D. P. Bertsekas, "Multiplier methods: a survey," *Automatica* **12**(2), 133–145 (1976).

18. M. Tao, J. Yang, and B. He, "Alternating direction algorithms for total variation deconvolution in image reconstruction," TR0918, Department of Mathematics, Nanjing University (2009).

19. W. Li, J. Yang, and Y. Huang, "Keystone transform-based space-variant range migration correction for airborne forward-looking scanning radar," *Electron. Lett.* **48**(2), 121–122 (2012).

20. M. A. Richards, *Fundamentals of Radar Signal Processing*, Tata McGraw-Hill Education, New York (2005).

21. M. Piles et al., "Spatial-resolution enhancement of SMOS data: a deconvolution-based approach," *IEEE Trans. Geosci. Remote Sens.* **47**(7), 2182–2192 (2009).

22. M. Cetin, "Feature-enhanced synthetic aperture radar imaging," PhD Thesis, University of Salford, Manchester, UK (2001).

23. D. Gabay and B. Mercier, "A dual algorithm for the solution of nonlinear variational problems via finite element approximation," *Comput. Math. Appl.* **2**(1), 17–40 (1976).

24. R. Glowinski and A. Marroco, "Sur l'approximation, par éléments finis d'ordre un, et la résolution, par pénalisation-dualité d'une classe de problèmes de dirichlet non linéaires," *ESAIM: Math. Modell. Numer. Anal.* **9**(R2), 41–76 (1975).

25. M. V. Afonso, J. M. Bioucas-Dias, and M. A. Figueiredo, "Fast image recovery using variable splitting and constrained optimization," *IEEE Trans. Image Process.* **19**(9), 2345–2356 (2010).

26. J. Eckstein and D. P. Bertsekas, "On the Douglas-Rachford splitting method and the proximal point algorithm for maximal monotone operators," *Math. Program.* **55**(1–3), 293–318 (1992).

27. M. V. Afonso, J. M. Bioucas-Dias, and M. A. Figueiredo, "An augmented Lagrangian approach to the constrained optimization formulation of imaging inverse problems," *IEEE Trans. Image Process.* **20**(3), 681–695 (2011).
28. S. Ramani and J. A. Fessler, "A splitting-based iterative algorithm for accelerated statistical x-ray CT reconstruction," *IEEE Trans. Med. Imaging* **31**(3), 677–688 (2012).
29. M. A. Figueiredo and J. M. Bioucas-Dias, "Restoration of Poissonian images using alternating direction optimization," *IEEE Trans. Image Process.* **19**(12), 3133–3145 (2010).
30. P. L. Combettes and V. R. Wajs, "Signal recovery by proximal forward-backward splitting," *Multiscale Model. Simul.* **4**(4), 1168–1200 (2005).
31. W. Yin et al., "Practical compressive sensing with Toeplitz and circulant matrices," in *Visual Communications and Image Processing 2010*, pp. 77440K, SPIE Press, Bellingham, Washington (2010).
32. Y.-M. Huang, M. K. Ng, and Y.-W. Wen, "A new total variation method for multiplicative noise removal," *SIAM J. Imaging Sci.* **2**(1), 20–40 (2009).
33. Z. Wang and A. C. Bovik, "Mean squared error: love it or leave it? A new look at signal fidelity measures," *IEEE Signal Process. Mag.* **26**(1), 98–117 (2009).

Yuebo Zha received his BS degree in applied mathematics and his MS degree in operation research from the University of Electronic Science and Technology of China in 2011, where he is currently working toward his PhD in signal and information processing.

Yulin Huang received his BS and PhD degrees in electronic engineering from the University of Electronic Science and Technology of China (UESTC), Chengdu, China, in 2002 and 2008, respectively. He is currently an associate professor with UESTC. His research interests include signal processing and radar imaging.

Jianyu Yang received his BS degree in electronic engineering from the National University of Defense Technology, Changsha, China, in 1984 and his MS and PhD degrees in electronic engineering from the University of Electronic Science and Technology of China (UESTC), Chengdu, China, in 1987 and 1991, respectively. He is currently a professor with the School of Electronic Engineering, UESTC. His research interests are mainly in synthetic aperture radar and signal processing.